An Approach on Thermal Analysis of 3-Phase Squirrel Cage Induction Motor

Mertcan KARAKUŞ[1], Güven ONUR[1], and Derya Ahmet KOCABAŞ[1]

[1]Istanbul Technical University, Istanbul, Türkiye
karakusm17@itu.edu.tr, onurgu@itu.edu.tr, derya.kocabas@itu.edu.tr

Abstract

For an induction motor to work efficiently, its losses must be low and, for a long service life, its windings must not be damaged. The most important factor that concerns these issues is heating. Analytical and numerical analysis of the sample induction motor were performed in this study using ANSYS RMxprt and Maxwell 2D software. Iterative electromagnetic and thermal analyses of the model were carried out in Motor-CAD software to ascertain the thermal behavior of the induction motor. The accuracy of the model has been tested with an experimental study and it has been found to have an accuracy of 97.3%.

1. Introduction

The aim to get the maximum power and torque density with the least amount of material has grown for electric motors. This requires the ability to generate substantial power and torque in a smaller volume. This can be achieved by reducing the size of the machine by using high quality materials. However, as the size of the machine decreases, the heating of the machine becomes more of a problem. Increased heat can damage the machine's insulation and cause the windings to short-circuit, potentially rendering the machine dysfunctional.

The lifespan of the insulation material is generally considered to be synonymous with that of the induction motor itself [1]. The most critical factor affecting the lifespan of the insulation material is temperature. For long-term smooth operation of the induction motor, the winding temperature must not exceed the insulation's maximum operating limit [2].

As it can be understood, thermal modeling holds equal importance with electromagnetic and mechanical modeling in terms of efficiency and operating lifespan in induction motor design. The maximum output power is set by its thermal analysis of the machine. Identifying the highest winding temperature points during start-up, overload, short-circuit operations and nominal operation through thermal analysis is critical for ensuring both insulation quality and machine longevity [3].

The purpose of this study is to conduct electromagnetic and thermal analyses to determine the thermal distribution in a sample three-phase squirrel cage 5.5 kW induction motor. In Section 2, general information and mathematical equations regarding the thermal analysis of an induction motor are given. In Section 3, the analyzes made in ANSYS RMxprt, Maxwell 2D and Motor-CAD programs are shown. In Section 4, the results and interpretations of the analyzes are presented. By the conclusion of this study, a flexible thermal design has been developed that can accurately predict the temperature distribution and thermal behavior of the sample three-phase squirrel-cage induction motor. This design can be modified, developed, and adapted to suit various conditions.

2. Thermal Analysis of An Induction Motor

Electrical energy is supplied to the stator of induction motors and is converted as mechanical power from the motor shaft. Thus, the motor converts electrical energy to mechanical energy. The path followed by the energy entering the stator windings is the air gap, rotor windings and shaft, respectively. Along this path, some energy is lost, resulting in less energy at the output than what was initially supplied to the stator. The difference between the energy supplied to the stator and the energy received at the output indicates the losses. It is possible to divide the losses into active power losses and reactive power losses. Active losses lead to an increase in temperature [4].

The active power losses of an induction motor can be generally divided into four headings: Copper losses, iron losses, mechanical losses and additional losses [5].

For a three-phase induction machine, copper losses occurring in the stator are calculated as in Equation (1). R_1 represents the resistance of the stator windings, I_1 represents the current passing through the stator windings and phase number is 3. Copper losses occurring in the rotor are calculated as in Equation (2). R_2' represents the resistance of the rotor windings reduced to the stator, and I_2' represents the current flowing through the rotor windings reduced to the stator [4].

$$P_{cu1} = 3R_1I_1{}^2 \qquad (1)$$

$$P_{cu2} = 3R_2{}'(I_2')^2 \qquad (2)$$

In an induction motor, copper losses increase as the rotor speed increases. In addition, as the temperature increases, the resistance values also increase [5].

Iron losses, which occur in alternating current, make up 25-30% of total losses. These losses increase in direct proportion to frequency and voltage. Iron losses can basically be divided into hysteresis losses and eddy current losses [4].

Mechanical losses, called friction and ventilation losses, vary approximately with the square of the rotor speed. Since the speed does not change much in induction motors, friction and ventilation losses are considered constant [4].

Like mechanical losses, additional losses are not represented in the T-equivalent circuit and are difficult to quantify. According to IEC standards, these losses constitute about 0.5% of the input power. They include the effects of load current harmonics and the losses due to the skin effect [6].

2.1. Heat Transfer in Induction Motor

The heat transfer mechanism network used for thermal analysis is analogous to an electrical circuit. For this analogy to be accurate, the thermal resistances in different parts of the motor must be calculated [5].

Heat transfer in electrical machines occurs in three ways: convection, conduction, and radiation, although radiation is usually negligible [1].

Conductive heat transfer is the primary mechanism in solid components like the rotor and stator. To model conduction, thermal conductivity λ (W/K.m) and conduction thermal resistance R_{th} parameters must be found. R_{th} (^{o}C/W) can be calculated as follows, where S is the heat transfer area and L is length [5].

$$R_{th} = \frac{L}{\lambda.S} \qquad (3)$$

Convection is the main mode of heat transfer for fluids, notably occurring in the air gap and between the stator surface and the motor frame. To model convection, heat transfer coefficient h (W/m^{2}K) and convection thermal resistance R_C (^{o}C/W) parameters must be found. R_C (^{o}C/W) can be calculated as follows, where A is the emitter surface area [1] [8].

$$R_c = \frac{L}{h \cdot A} \qquad (4)$$

2.2. Thermal Models in Induction Motor

Thermal models are used in electrical machines to examine the thermal behavior of the machine and to extract the temperature distribution. Various methods are used in the thermal modeling of induction motors, including lumped parameter models, shell models, FEM models, and models based on fluid dynamics [1].

In the lumped parameter modeling type, the relevant electrical machine is divided into geometrical subunits. The thermal resistance and thermal capacity of each subunit are determined utilizing an analogy between thermal quantities and electrical quantities. When simulating electrical quantities, it should be considered that each subunit acts as a heat source and therefore has thermal capacity and has thermal resistance with other elements of the machine [5]. During these calculations, it's essential to identify the heat transfer mechanism—either conduction or convection—for each subunit. Then, the thermal capacity and resistance values found are combined in accordance with the geometry of the machine and the electrical equivalent circuit of the machine, which describes the thermal behavior, is obtained. The circuit can be solved using Kirchoff's laws [1]. Some assumptions are made in the lumped parameter modeling method. Some assumptions in this method include radial and shaft axial symmetry of the machine, negligible ambient heat transfer, uniform heat source distribution, and the existence of a single average temperature value [6]. The similarity table between electrical and thermal properties is given in Table 1.

Table 1. Analogy between electrical and thermal quantities [5]

Thermal Quantity	Sym	Unit	Electrical Quantity	Sym	Unit
Temperature	T	K	Electrical potential	V	V
Temperature rise	Θ	K	Voltage	U	V
Heat flow rate	Φ_{th}	W	Current	I	A
Thermal capacity	C_{th}	J/K	Capacity	C	F
Thermal resistance	R_{th}	K/W	Resistance	R	Ω

In the established lumped parameter thermal equivalent circuit, the heat source is modeled at the nodes where there are losses. The thermal capacity is added to the necessary nodes by simulating the electrical capacity. The following equations are used to find the thermal capacity.

Thermal capacity C_{th} can be found as in Equation (5). Here, m is the mass of the object, c_p is the specific heat capacity [5].

$$C_{th} = m \cdot c_p \qquad (5)$$

When adapting the lumped parameter model to an induction motor, the induction motor is usually divided into ten sub-parts. These are: motor frame, stator yoke, stator teeth, stator winding, end windings, air gap, cover gap air, rotor winding, rotor iron and shaft. Air gap and cover space air do not have thermal capacity. Each subpart is modeled basically as a cylinder [5].

An example thermal equivalent circuit of the induction motor is shown in Figure 1. Since the majority of the motor's iron losses occur in the stator yoke, stator's copper losses in the stator winding, and rotor's copper losses in the rotor winding, thermal nodes are specially added to these parts [6] [10].
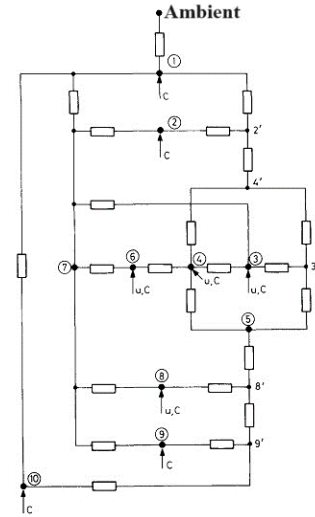

Fig. 1. Thermal equivalent circuit of an induction motor [6]

3. Design and Simulations

In this section, the electromagnetic analysis of the sample motor will be performed first, followed by the thermal analysis, and the simulation results will be compared to the test results.

Analytical analysis with ANSYS Rmxprt software will be performed initially, followed by numerical analysis utilizing FEM with ANSYS Maxwell 2D. Thermal analysis will be performed with Motor-CAD software.

The motor to be analyzed is a 5.5 kW three-phase squirrel cage Totally Enclosed Fan-Cooled (TEFC) induction motor with an IE3 energy efficiency class and a B3. It features 36 stator slots, 28 rotor slots and 2 poles.

3.1. Electromagnetic Analysis

The stator windings are single layer and have full corrugated winding type. The number of parallel branch is one. Since the motor has a three-phase two-pole structure with 36 slots, the number of slots per phase and pole (q_1) is calculated as 6.

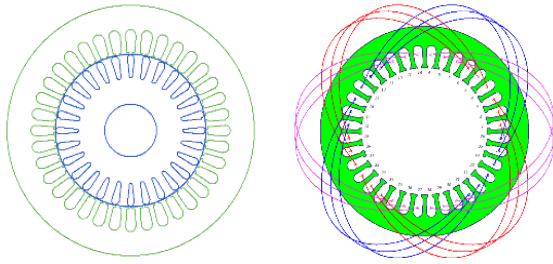The stator geometry and winding diagram are shown in Fig. 2.

Fig. 2. Stator geometry and winding diagram of the motor

The plate values of the sample motor to be used in the simulation program are given in Table 2.

Table 2. Initial values for sample motor

Parameter	Value
Installation type	Constant power
Rated output power	5500 W
Rated voltage	660 V
Frequency	50 Hz
Rated speed	2920 min^{-1}
Winding connection method	Star

RMxprt and Maxwell 2D using finite element method were used for electromagnetic analysis. Internal mechanical power is calculated as the output power in the Maxwell 2D program, and mechanical losses and additional losses are not included. In Maxwell 2D, meshes were assigned for FEM, eddy current losses and core losses were also assigned and simulation was run.

The electromagnetic analysis results are given in Table 3.

Table 3. Comparison of RMxprt and Maxwell 2D results

Parameter	Motor Data	RMxprt	Diff.	Maxwell 2D	Diff.
Output power	5500W	5500.3W	~ 0	5774W	4.98%
Speed (rpm)	2920	2917.45	0.09%	2917.45	0.09%
Line current	9.5 A	9.66 A	1.6%	9.63 A	1.36%
Torque	18 Nm	18 Nm	~ 0	18.77 Nm	4.27%
Efficiency	88.5%	88.3%	~ 0	94.4%	6.67%
Input power	6247 W	6229W	0.29%	6116W	2.09%

3.2. Thermal Analysis

Motor-CAD software was used for thermal analysis of the sample motor. Iterations are made between electromagnetic and thermal analysis. Iterative processes were conducted between the electromagnetic and thermal analyses, with feedback from the thermal analysis used to optimize design parameters. These iterations take into account temperature effects that affect electromagnetic performance. It is aimed to obtain realistic results by modeling the cooling fan, motor frame, motor mount and cover chamber in Motor-CAD.

Thermal resistances and capacities can be auto-calculated in Motor-CAD using motor dimensions and material data.

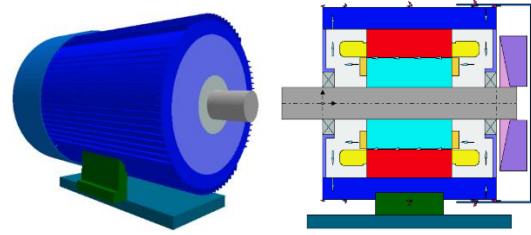The sample motor is transferred to Motor-CAD and its model is illustrated in Figure 3.

Fig. 3. 3D and axial Motor-CAD model of the motor

In the simulation of the cooling system, motor geometry and material data are employed to compute the air circulation rate around the motor. Additionally, the convection heat transfer coefficient, denoted as h, can be manually input for the frame's fins. It is crucial to input h coefficients for various motor surface areas to account for both natural and forced convection. The motor features a self-ventilating cooling system, making it necessary to provide h coefficients for regions with internal air circulation. Using experimental data for these calculations enhances result accuracy. The outdoor temperature was set at 23.7°C, aligning with the experimental conditions.

After the necessary inputs were entered, the simulation was run in which electromagnetic and thermal analysis would be integrated in iterations.

4. Results and Interpretation

In this section, an experimental study will be carried out to determine the temperature distribution of a 5.5 kW sample motor.

During the experimental study, thermocouples were placed in various parts of the induction motor: Air gap, upper middle part of the frame, front and rear bearing, front and rear stator end windings. Experimental environment was 23.7 °C and the initial winding temperature is considered equal to this value.

The experimental setup is given in Figure 4.

Fig. 4. Experimental setup

After the thermocouples were placed, the motor was powered and started. While the motor was running at full load, output power, voltage and current values were measured with the help of measuring devices.

To obtain the heating curves, 1634 temperature measurements were taken at 6-second intervals for 9835 seconds (163.9 minutes) with thermocouples placed on the induction motor. These measurements were used to determine heating curves for various parts of the motor.

The comparison of calculated and measured electromagnetic results are given in Table 4.

Table 4. Calculated and experimentally measured values

Parameter	Experiment	RMxprt	Diff.	Motor-CAD	Diff.
Output power	5530 W	5500.3 W	0.54%	5504.3	0.46%
Input Power	6247 W	6229W	0.29%	6269.4	0.36%
Speed (rpm)	2920	2917.45	0,09%	2920	~ 0
Line current	10.2 A	9.66 A	5.3%	9.9	2.94%
Torque	18 Nm	18 Nm	~ 0	18	~ 0
Power coefficient	0.89	0.95	6.74%	0.91	2.25%
Efficiency	88.5%	88.3%	0.22%	87.79%	0.8%

Loss values in watts were calculated using the parameters measured in the experiment. These values are given in Table 5.

Table 5. Calculated and experimentally measured losses

Loss	Experiment	RMxprt	Diff.	Motor-CAD	Diff.
Stator copper	277	279.31	0.83%	270.7	2.27%
Rotor copper	158	157.04	0.60%	154.9	1.96%
Iron	145	143.51	1.03%	154.6	6.62%
Additional	91.36	99	8.36%	133.2	45.8%
Fric. and Vent	46.07	49.91	8.33%	50.12	8.77%

It can be observed in Table 5 that the RMxprt analysis provides more accurate results. The biggest differences are seen in additional losses and friction and ventilation losses. In particular, the additional losses of 133.2 W calculated in the Motor-CAD analysis are far from the measured value (91.36 W). There can be several reasons for this. It was mentioned in previous sections that additional losses are difficult to calculate. They include the effects of load current harmonics and losses due to skin effect.

4.1. Thermal Results

In this section, the heating data obtained through experiments will be compared with the data calculated in the Motor-CAD. Temperature distribution calculated with Motor-CAD is as follows.
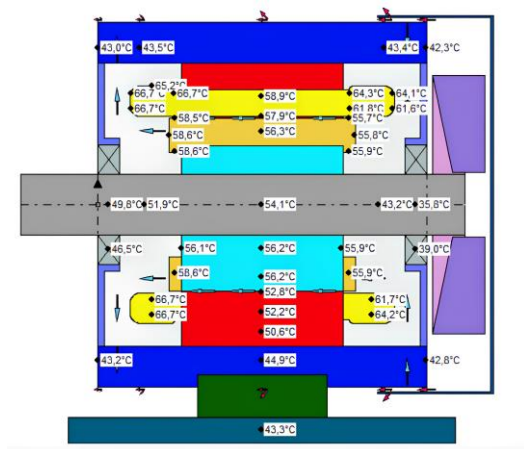

Fig. 5. Temperature results obtained in Motor-CAD (axial view)

In steady state, the measured and calculated values of temperatures in different parts of the motor are given in Table 6.

Table 6. Comparison of calculated and experimentally measured temperatures in steady state

Region	Experiment	Motor-CAD	Difference
Stator rear end winding	64.075 °C	64.1 °C	0.04%
Stator front end winding	65.871 °C	66.7 °C	1.26%
Rear bearing	38.356 °C	39.0 °C	1.68%
Front bearing	50.221 °C	46.5 °C	7.4%
Air gap	58.198 °C	57.9 °C	0.51%
Upper frame midsection	41.309 °C	43.5 °C	5.3%

Table 6 shows that there is an acceptable degree of agreement between the experimental and Motor-CAD analysis results. In the experiment, the hottest part of the motor is the stator end winding at the front, that is, on the load side, as in the Motor-CAD analysis. In the experiment, the temperature here is 65.871°C, and in the analysis, it is 66.7°C. The difference is 1.26%. In addition, the difference for the rear end winding is 0.04%. Air gap temperature could be calculated with a deviation of 0.51%.

As can be seen in Table 6, the front parts of the motor are hotter than the rear parts due to the location of the fan.

Comparative representations of the curves obtained in the Motor-CAD and those obtained in the experiment are given below. Curves were extracted using MATLAB.
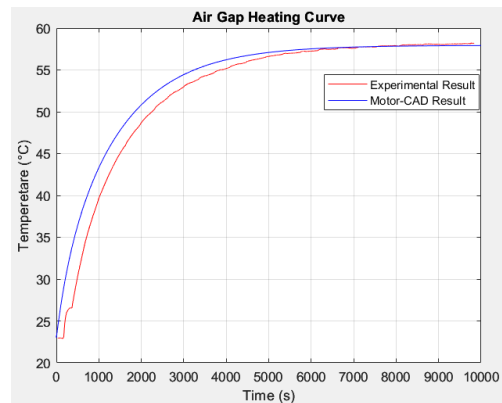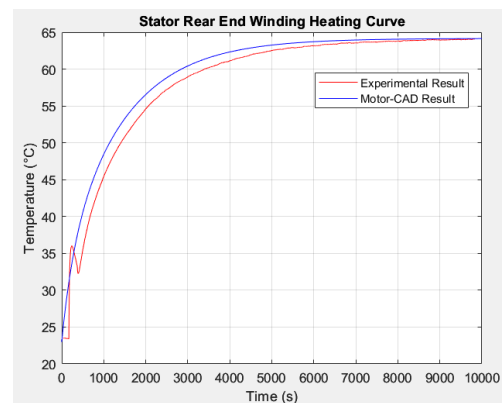

Fig. 6. Air gap heating curve

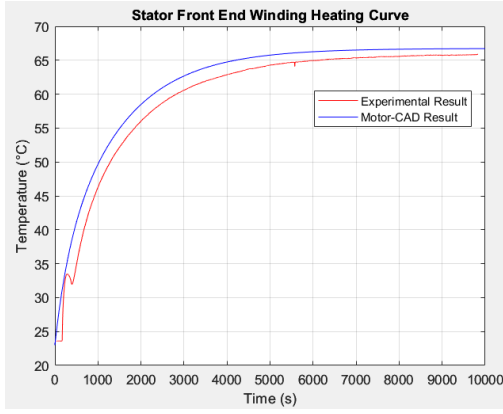**Fig. 7.** Stator rear end winding heating curve

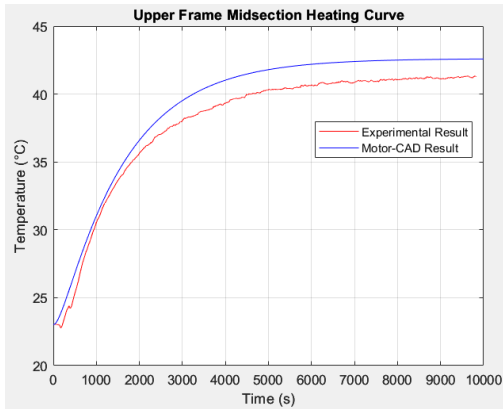**Fig. 8.** Stator front end winding heating curve

Fig. 9. Upper frame midsection heating curve

When the heating curves are compared with the Motor-CAD analysis results, it can be seen that they are reasonably compatible with each other. In all the graphs given, measured and calculated heatings exhibit similar movements and the time for the temperature to settle to the steady state value is approximately the same.

In order to examine the effect of material change on temperature, the simulation was performed again by selecting iron instead of aluminum for the motor frame in Motor-CAD and Table 7 was obtained. From this analysis, it can be generally said that the temperature of the motor has increased. Therefore, using iron instead of aluminum in the motor frame causes temperature increases in many parts of the motor. The biggest reason for this is that the thermal conductivity of iron (180 W/mK) is higher than aluminum (80 W/mK).

Table 7. Calculated temperatures when the motor frame is iron and aluminum

Region	With Iron	With Aluminum
Stator rear end winding	65.8 °C	64.1 °C
Stator front end winding	68.7 °C	66.7 °C
Rear bearing	39.0 °C	39.0 °C
Front bearing	46.2 °C	46.5 °C
Air gap	60.2 °C	57.9 °C
Upper frame midsection	42.6 °C	43.5 °C

5. Conclusions

As a result, this study was conducted using RMxprt, Maxwell 2D and Motor-CAD programs to determine the thermal behavior of a sample 5.5 kW three-phase cage general purpose induction motor. By using numerical analysis methods to examine analytical and magnetic effects, a thermal design was obtained that can be adapted, modified and further developed to suit different conditions. For this purpose, electromagnetic and thermal analyzes were performed simultaneously in iterations. The accuracy of the design was tested with experimental studies and it was found to have an accuracy rate of 97.3%. Thus, heating in various parts of the motor before and/or after production can be predicted more easily and quickly, without the need for difficult and time-consuming experimental studies. In the experimental study, there are regions where thermocouples cannot be placed. These are rotor bars and rotor yoke. The fact that the temperature distribution calculated with the generated thermal model is compatible with the stator windings and many other parts of the motor means that the temperature values in the rotor can be calculated approximately accurately.

In addition, the materials used for the induction motor can be tested in the model to monitor the thermal behavior of the motor and optimize the temperature distribution.

For more precise results, 3D analyzes can be performed in programs that use FEM and include fluid dynamics analysis such as ANSYS Fluent.

6. References

[1] Gürgöze, F., Kafesli Asenkron Motorların Dinamik Isıl Modeli, *Master Thesis*, Istanbul Technical University, Istanbul, 2002.

[2] Mergen, A. F., Kocabaş, D. A., "Elektrik Makinalarında Sargılar," Birsen Yayınevi, İstanbul, 2007.

[3] Boldea, I., Nasar, S., "The Induction Machines Design Handbook (2nd edition)," CRC Press, New York, 2010.

[4] Mergen, A. F., Zorlu, S., "Elektrik Makineleri 2 Asenkron Makineler," Birsen Yayınevi, İstanbul, 2009.

[5] Pyrhönen, J., Jokinen, T., Hrabovcova, V., "Design of Electrical Machines," John Wiley & Sons, Hoboken, New Jersey, 2008.

[6] Salman, E., Üç Fazlı Sincap Kafesli Asenkron Motorun Sıcaklık Dağılımının Çıkarılması, *Master Thesis*, Istanbul Technical University, İstanbul, 2011.

[7] Kocabaş, D. A., Asenkron Makinalarda Uzay Harmoniklerinin Etkilerini Azaltmaya Katkılar, *Doctoral Thesis*, İstanbul Teknik Üniversitesi, İstanbul, 2004.

[8] Gürdal, O., "Elektrik Makinalarının Tasarımı," Bursa Orhangazi Üniversitesi Yayınları, Bursa, 2015.

[9] Sarıkaya, P., Kafesli Asenkron Makinede Isınmanın İncelenmesi ve Isısal Devre Modelinin Kurulması, *Master Thesis*, Istanbul Technical University, İstanbul, 1999.

[10] Gürgöze, F., Mergen A. F., "Üç Fazlı Asenkron Motorlarda Sıcaklık Dağılımının Çıkartılarak Tasarım Optimizasyonunun Yapılması," *itü dergisi*. Cilt 9, sayı 1, ss. 36-44, 2010.